

RESEARCH

Open Access



Salidroside enhances NO bioavailability and modulates arginine metabolism to alleviate pulmonary arterial hypertension

Junfei Li¹, Zengyu Zhang¹, Chenghui Zhu², Xiaorong Zheng¹, Chunlei Wang¹, Jianwei Jiang^{1*} and Hongyan Zhang^{1*}

Abstract

Background Salidroside (SAL), derived from Rhodiola, shows protective effects in pulmonary arterial hypertension (PAH) models, but its mechanisms are not fully elucidated.

Objectives Investigate the therapeutic effects and the mechanism of SAL on PAH.

Methods Monocrotaline was used to establish a PAH rat model. SAL's impact on oxidative stress and inflammatory responses in lung tissues was analyzed using immunohistochemistry, ELISA, and Western blot. Untargeted metabolomics explored SAL's metabolic regulatory mechanisms.

Results SAL significantly reduced mean pulmonary artery pressure, right ventricular hypertrophy, collagen deposition, and fibrosis in the PAH rats. It enhanced antioxidant enzyme levels, reduced inflammatory cytokines, and improved NO bioavailability by upregulating endothelial nitric oxide synthase (eNOS), soluble guanylate cyclase (sGC), cyclic guanosine monophosphate (cGMP), and protein kinase G (PKG) and decreases the expression of endothelin-1 (ET-1). Metabolomics indicated SAL restored metabolic balance in PAH rats, particularly in arginine metabolism.

Conclusions SAL alleviates PAH by modulating arginine metabolism, enhancing NO synthesis, and improving pulmonary vascular remodeling.

Keywords Salidroside, Pulmonary artery hypertension, Arginine metabolism, NO bioavailability

Introduction

Pulmonary arterial hypertension (PAH) is a chronic pulmonary circulatory disorder, with a prevalence rate as high as 10% among individuals over the age of 65 [1, 2].

It is predominantly characterized by abnormal constriction of pulmonary vessels, luminal narrowing, and vascular remodeling, and eventually develops into irreversible right heart failure, posing a significant threat to human health [3]. Regrettably, curative treatments for PAH are still lacking at present. Therefore, finding feasible measures to delay or halt the progression of PAH is crucial.

The pathogenesis of PAH is multi-factorial, complex and not fully understood. The reduced synthesis and bioavailability of nitric oxide (NO) in pulmonary vascular tissue serve as key drivers of PAH [4]. NO is produced by endothelial cells, diffuses through the endothelium to the smooth muscle, and mediates vasodilation via

*Correspondence:

Jianwei Jiang

jiangjw@zjcc.org.cn

Hongyan Zhang

zhanghy@zjcc.org.cn

¹ Zhejiang Cancer Hospital, Hangzhou Institute of Medicine and Cancer (HIM), Chinese Academy of Sciences, 1# Banshan east Road, Gongshu District, Hangzhou CN 310022, Zhejiang, China

² Wannan Medical College, Wuhu 241000, Anhui, China



the soluble guanylate cyclase (sGC)-cyclic guanosine monophosphate (cGMP)-protein kinase G (PKG) pathway. Insufficient NO causes impaired pulmonary vascular dilation, oxidative stress, and inflammation, causing vascular wall thickening and the progression of PAH [5]. Thus, enhancing the release and bioavailability of NO in the pulmonary arteries of PAH patients is a focus of current research.

Rhodiola is a traditional Chinese medicine from the Tibetan area and has been used to treat vascular diseases and various diseases caused by hypoxic environments for thousands of years. Salidroside (SAL), the main active component of Rhodiola, can promote NO release and upregulate the bioavailability, dilate blood vessels to alleviate vascular plaques and endothelial dysfunction, ameliorating the symptoms of arteriosclerosis model rats [6–8]. Previous studies found that SAL can alleviate symptoms in PAH model mice by regulating the proliferation and apoptosis of pulmonary arterial vascular smooth muscle cells [9, 10]. However, there are no reports clarify whether SAL improves pulmonary vascular endothelial dysfunction and treats PAH by increasing the synthesis and bioavailability of NO.

In this study, we observed the therapeutic effects of SAL on PAH model rats using multiple methods, and evaluated the improvements in oxidative stress and inflammatory in lung tissue via enzyme-linked immunosorbent assay (ELISA) and real-time reverse transcription quantitative polymerase chain reaction (RT-qPCR). Then, we examined the expression of key factors reflecting the synthesis and bioavailability of NO in the pulmonary artery, and applied an untargeted metabolomics approach to elucidate the metabolism of SAL's anti-PAH action.

Materials and methods

Reagents

SAL (CAS: 10338–51-9, HY-N0109), purity > 99.79%, was purchased from MedChemExpress. monocrotaline (MCT; CAS: 315–22-0, WKQ-0000641), purity ≥ 98.00%, was obtained from Sichuan Weikeqi Biological Technology Co., Ltd (Chengdu, China). The Superoxide Dismutase (SOD) assay kit (WST-1 method, A001-3–2), Malondialdehyde (MDA) assay kit (TBA method, A003-1–2), Glutathione Peroxidase (GSH-PX) assay kit (Colorimetric method, A005-1–2), and NO assay kit (Nitrate reductase method, A012-1–2) were purchased from Nanjing Jiancheng Biological Engineering Institute (Nanjing, China). BCA Protein assay kit (ml095490), interleukin (IL)-1 β (ml003057), tumor necrosis factor- α , (TNF- α , ml002859), IL-6 (ml102828), and cGMP (ml003133) ELISA kits were acquired from Shanghai Enzyme-linked Biotechnology Co., Ltd. (Shanghai,

China). α -smooth muscle actin (α -SMA) antibody (ab7817, 1:500) was sourced from Abcam Inc. (Shanghai, China). Total RNA extraction, first-strand cDNA reverse transcription, polymerase chain reaction (PCR) kits, and primers were obtained from TianGen Biotechnology Co., Ltd. (Beijing, China). Endothelial nitric oxide synthase (eNOS) antibody (27120–1-AP, 1:1000), PKG antibody (21646–1-AP, 1:1000) were purchased from Proteintech Group, Inc. (Hubei, China); sGC antibody (ab225864, 1:1000) and endothelin-1 (ET-1) antibody (ab2786, 1:500) were bought from Abcam Inc. (Shanghai, China).

Animals and treatment

Following the method of Arifin WN et al. [11], the sample size for animal experiments was determined to be 6 per group. Therefore, 30 SPF-grade SD rats, male, aged 6 weeks, weighing 200 ± 20 g, were purchased from SLAC Animal Inc. (Shanghai, China). All procedures of Animal experiments were carried out in accordance with the “Guidelines for the Management and Use of Laboratory Animals (China)” and were approved by the Animal Experiment Ethics Committee of Zhejiang Cancer Hospital. All methods were reported in accordance with ARRIVE guidelines. Rats were housed in plastic cages within an SPF barrier, with a 12-h light/dark cycle, at a temperature of 22 ± 2 °C and humidity of $45 \pm 10\%$. After a week of acclimatization, the 30 rats were randomly divided into five groups: Control, Model, Sildenafil (SLD), Low Dose SAL (LD-SAL), and High Dose SAL (HD-SAL). SLD, a commonly used clinical drug for treating PAH, served as the positive control in this experiment. Rats in the Model, SLD, LD-SAL, and HD-SAL groups were given a single subcutaneous injection of MCT (60 mg/kg) to establish the PAH model. The Control group was injected subcutaneously with an equivalent volume of saline. From the day of MCT injection, the SLD group was administered SLD (30 mg/kg) daily by gavage, the LD-SAL and HD-SAL groups received SAL at 25 mg/kg/d and 50 mg/kg/d, respectively, by gavage, and the Control group was given an equivalent volume of saline by gavage for 4 weeks.

Pulmonary arterial pressure measurement

Rats were anesthetized with 3% pentobarbital sodium (45 mg/kg) by intraperitoneal injection. A right neck incision was made, exposing the external jugular vein, and a 2–3 mm “V” shaped incision was made towards the heart. A microcatheter was inserted and connected to a pressure sensor linked to a Powerlab physiological recorder. The catheter was advanced to the pulmonary artery to measure mean pulmonary arterial pressure (mPAP). After recording, euthanasia was performed under anesthesia.

Cardiac-related indices measurement

Rat hearts were extracted and weighed, the right ventricular free wall (RV) was separated along the interventricular septum, and the remaining part was designated as the left ventricle and septum tissue (LV+S). After drying, the weights of RV and LV+S were measured, and the Right Ventricular Index (RVI; RVI=[RV (mg)/BW (g)]), Right Ventricular Hypertrophy Index (RVHI; RVHI=[RV/(LV+S)]), and Cardiac Index (CI; CI=[HW/BW]) were calculated.

Histological examination

Lung tissues were sectioned, fixed in 4% paraformaldehyde, dehydrated overnight, and embedded in paraffin. 5 µm Sections were cut for H&E and Masson staining. A computer image analysis system was used to measure pulmonary arterioles of about 100 µm, and Leica Qwin analysis software calculated the mean vascular Total Area (TA) and vascular lumen Area (IA) of pulmonary arterioles. The percentage of pulmonary arteriole Wall Area in total vascular area (WA%; WA%=[(TA-IA)/TA × 100%]) was calculated. The expression of α-SMA in lung tissues was determined by immunohistochemistry, stained with 3, 3'-Diaminobenzidine Tetrahydrochloride for substrate chromogen, and counterstained with hematoxylin. In Masson staining, the blue areas represent collagen, and in immunohistochemistry staining, the brown-red areas indicate α-SMA expression. ImageJ software analyzed images from Masson and immunohistochemistry stained sections to calculate the Area Optical Density (AOD; AOD=[IOD/(Area/Per Area)]), where IOD is the integrated optical density.

ELISA for cytokines

The levels of IL-1β, IL-6, and TNF-α in lung tissues, and cGMP level in pulmonary artery tissue were measured using ELISA kits according to the manufacturer's instructions.

Assay kit detection

The levels of SOD, MDA, and GSH-PX in lung tissues, and NO level in pulmonary artery tissue were measured using relative commercial kits according to the manufacturer's instructions.

qPCR detection

Total RNA was isolated from rat lung tissues using an RNA extraction kit. According to the instructions, 1 µg of total RNA was used for first-strand cDNA synthesis. The expression of IL-1β, IL-6, and TNF-α was detected by RT-qPCR, with all samples run in triplicate using

the BioRad iQ5 system. β-Actin served as the control. Quantification was performed using the $2^{-\Delta\Delta CT}$ method. Primer sequences are shown in Table 1.

Western blot analysis

Three rats were randomly selected from each group, and their pulmonary arteries were minced. After lysis and centrifugation, the supernatant was collected, and the protein concentration was determined by the BCA method. SDS-PAGE gel was prepared for electrophoresis and transferred onto a PVDF membrane. The membrane was blocked with 5% BSA. Primary antibodies were added and incubated overnight at 4 °C. Then, secondary antibodies were incubated at 37 °C for 2 h. The PVDF membrane was placed in a gel imaging analysis system for imaging. β-Actin protein was used as an internal reference, the gray value of the bands was quantified using Image J software.

Untargeted metabolomics study

Six rats were randomly selected from each group to obtain the pulmonary artery tissue homogenate, as described in 2.9. Liquid chromatography–mass spectrometry (LC–MS) technology was used to screen for metabolite changes in the tissue homogenate after 28 days of SAL treatment. The following sections detail LC–MS detection and data analysis protocols.

Chromatography and mass spectrometry conditions

Chromatography was performed using a Hypesil Gold column (C18) (2.1 mm×100 mm, 1.9 µm), with the mobile phase consisting of (A) 0.1% formic acid and (B) methanol, using a gradient elution. The gradient started at 98% A and 2% B at 0 min, held until 1.5 min, changed to 0% A and 100% B by 12 min, held until 14 min, then returned to 98% A and 2% B at 14.1 min, and held until 17 min. The column temperature was set at 40 °C, with a flow rate of 0.2 mL/min, and the injection volume was 2 µl. Mass spectrometry conditions included an

Table 1 Primer sequence of target genes for rats

Genes	Primer sequence (5'-3')
β-actin	Forward: GGTGGGAATGGGTCAAGAAGG Reverse: TGGCCTTACGGTTCAAGGGG
IL-1β	Forward: AATGCCACCTTTGACAGTGA Reverse: GCAGCCCTTCATCTTTGGG
IL-6	Forward: CCCAATTCCAATGCTCTCC Reverse: GGATGGTCTGGTCCTAGCC
TNF-α	Forward: ATGCCCTCCCTCATCAGT Reverse: TTTGCTACGACGTGGGCTAC

electrospray ionization source in both positive and negative ion modes. The ESI source settings were: Spray Voltage: 3.2 kV; Sheath gas flow rate: 40 arb; Aux Gas flow rate: 10 arb; Capillary Temp: 320 °C; scanning range m/z 100–1500; MS/MS scans were data-dependent.

Data processing and analysis

Molecular feature peaks in the samples were detected based on High Resolution Mass Spectrometry (HRMS) technology. Initial screening was performed based on a retention time and mass-to-charge ratio, followed by peak alignment across different samples with a retention time deviation of 0.2 min and mass deviation (Part per million, ppm) of 5 ppm. Peaks were then extracted based on set criteria including a 5 ppm, a signal intensity deviation of 30%, a signal-to-noise ratio (S/N) of 3, minimum signal intensity of 100,000, and adduct ions, and peak areas were quantified. Molecular formulas were predicted based on molecular ion peaks and fragment ions, and compared against mzCloud (<https://www.mzcloud.org/>), mzVault, and MassList databases for metabolite identification. Metabolites with a Coefficient of Variance (CV) less than 30% in QC samples were retained as final identification results for subsequent analysis. Compound Discoverer 3.1 (CD3.1, Thermo Fisher) software was used to integrate chromatographic peaks detected in samples, where each feature peak's area represented a relative quantitation of a metabolite, and total peak area normalization was performed. Multivariate statistical analysis, including principal component analysis (PCA) and partial least squares discriminant analysis (PLS-DA), was conducted to reveal metabolic pattern differences between groups. Potential biomarkers were selected based on $P \leq 0.05$ and VIP (Variable importance of projection) > 1 . Differential metabolites with Fold Change (FC) > 1.25 or FC < 0.80 underwent metabolic pathway enrichment analysis based on KEGG data (<https://www.kegg.jp/>).

Statistical analysis

All values are expressed as the mean \pm SD. The Student's *t* test was used for comparison between groups and one-way ANOVA for comparison among multiple groups. A value of $p < 0.05$ was considered to indicate a significant difference. GraphPad Prism 8.0 was used to analyze all statistical data.

Results

Effects of SAL on MCT-induced PAH model rats

The efficacy of SAL in the treatment of PAH was evaluated by measuring mPAP, the cardiac-related indices, and the condition of pulmonary vascular remodeling. The mPAP in the model group was significantly higher

than that in the control group ($p < 0.01$, Fig. 1A). After 4 weeks of SAL or SLD administration, the mPAP of the PAH model rats decreased ($p < 0.05$, Fig. 1A). MCT treatment led to significant increases in the cardiac-related indices (RVI, RVHI and CI) compared with the control group ($p < 0.01$, Fig. 1B), indicating right ventricular hypertrophy. Meanwhile, HD-SAL or SLD treatment alleviated right ventricular hypertrophy in the model group ($p < 0.05$, Fig. 1B).

The condition of pulmonary vascular remodeling in model rats was evaluated through the application of H&E and Masson staining, along with immunostaining. H&E staining and WA% indicated that the model group had thickened vascular walls and narrowed lumens compared with the control group, while SAL treatment led to enlarged luminal spaces and thinner vessel walls ($p < 0.01$, Fig. 2A, D). Masson staining disclosed collagen deposition around the vessels in PAH model rats, and significant reductions were observed after SAL treatment ($p < 0.01$, Fig. 2B, E). Immunostaining demonstrated that the α -SMA (markers of myofibroblasts) level in the model group was higher than in the control group. SAL treatment reduced the expression of α -SMA compared to the model group ($p < 0.01$, Fig. 2C, F). Overall, these results suggest that SAL has a therapeutic effect on pulmonary vascular remodeling in PAH model animals, and more pronounced effects were witnessed in the HD-SAL group.

Effects of SAL on oxidative stress and inflammation in PAH model rats

The impact of SAL on oxidative stress was investigated by measuring MDA, SOD, and GSH-PX levels using relative assay kits. Compared with the control group, MDA levels increased ($p < 0.01$), while the levels of SOD and GSH-PX decreased in the model group ($p < 0.05$). MDA levels decreased ($p < 0.01$), and SOD and GSH-PX levels increased ($p < 0.05$) in the HD-SAL group compared to the model group (Fig. 3A, B). The anti-inflammatory responses were examined by detecting IL-1 β , IL-6, and TNF- α levels in the lung tissues homogenate via ELISA and RT-qPCR. The protein and gene transcription levels of IL-1 β , IL-6, and TNF- α were upregulated in the model group compared to the control group ($p < 0.05$), while SAL intervention downregulated them ($p < 0.05$), with stronger effects in the HD-SAL group ($p < 0.01$) (Fig. 3C, D).

Effect of SAL on NO synthesis and bioavailability in the pulmonary artery tissue of PAH model rats

The above results confirmed that SAL has a significant therapeutic effect on PAH, with a stronger effect at a high dose. We chose the Control, Model, and HD-SAL

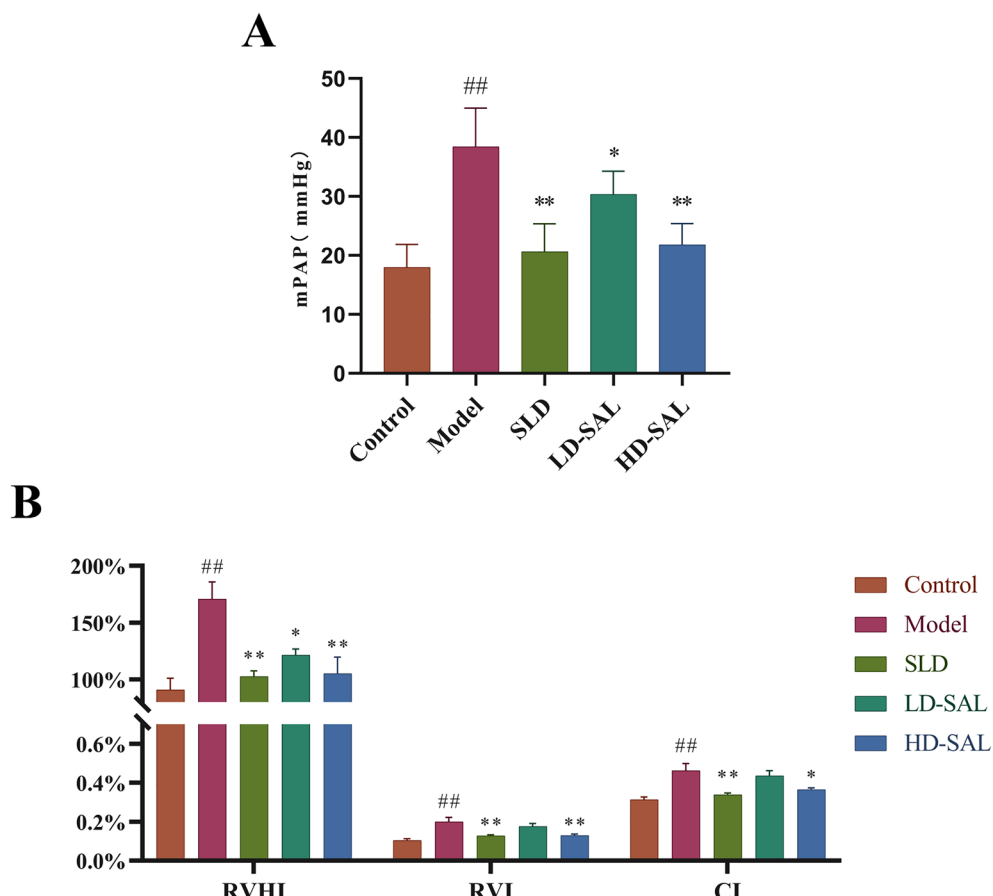


Fig. 1 Salidroside (SAL) treatment attenuates pulmonary arterial hypertension and right ventricular hypertrophy in MCT-induced PAH rats. **A** Mean pulmonary arterial pressure (mPAP) in the five experimental groups. **B** Cardiac-related indices: right ventricular hypertrophy index (RVHI), right ventricular index (RVI), and cardiac index (CI). Data are presented as mean \pm SD ($n=6$ per group). One-way ANOVA with Tukey's post hoc test was used for statistical analysis. * $P<0.05$, ** $P<0.01$ vs Model group; # $P<0.01$ vs Control group

groups for studies to further explore the effect of SAL on NO Synthesis and bioavailability in the pulmonary artery homogenate. We measured the expression of eNOS and NO to evaluate NO synthesis, and that of sGC, PKG, cGMP, and ET-1 to assess NO bioavailability. Compared with the control group, the levels of eNOS and NO decreased ($p<0.01$, Fig. 4A, C, D), the sGC–cGMP–PKG pathway was inhibited ($p<0.01$, Fig. 4B, C, D), and the expression of ET-1 protein was upregulated ($p<0.01$, Fig. 4D) in the model group. After SAL intervention, the levels of eNOS ($p<0.05$) and NO ($p<0.01$) increased (Fig. 4A, C, D), the sGC–cGMP–PKG pathway was activated ($p<0.05$, Fig. 4B, C, D), and the expression of ET-1 protein was down-regulated ($p<0.01$, Fig. 4D) compared with the model group. This indicates that SAL enhances the synthesis and bioavailability of NO in the pulmonary artery of model rats, thereby exerting vasodilatory and anti-PAH effects.

Effects of SAL on the metabolic mechanism in the pulmonary artery tissue of PAH model rats

We compared metabolite changes in the pulmonary artery tissue of the Control, Model, and HD-SAL groups using untargeted metabolomics. PCA and PLS-DA analyses revealed significant differences in metabolites between the Model group and the Control group, as well as between the HD-SAL group and the Control group. Compared with the Control group, the Model group had $R^2=0.75$, $Q^2=-0.86$; compared with the Model group, the HD-SAL group had $R^2=0.88$, $Q^2=-0.83$ (Fig. 5A–E).

Differential metabolites were selected based on the criteria of ion variable importance in projection (VIP) > 1 , $P < 0.05$, and fold change (FC) > 1.2 or FC < 0.8 , identifying 39 differential metabolites across the Control, Model, and HD-SAL groups. Metabolomic analysis of the differential metabolic pathways revealed 13 differential metabolites that enriched themselves into six related metabolic pathways among the Control, Model,

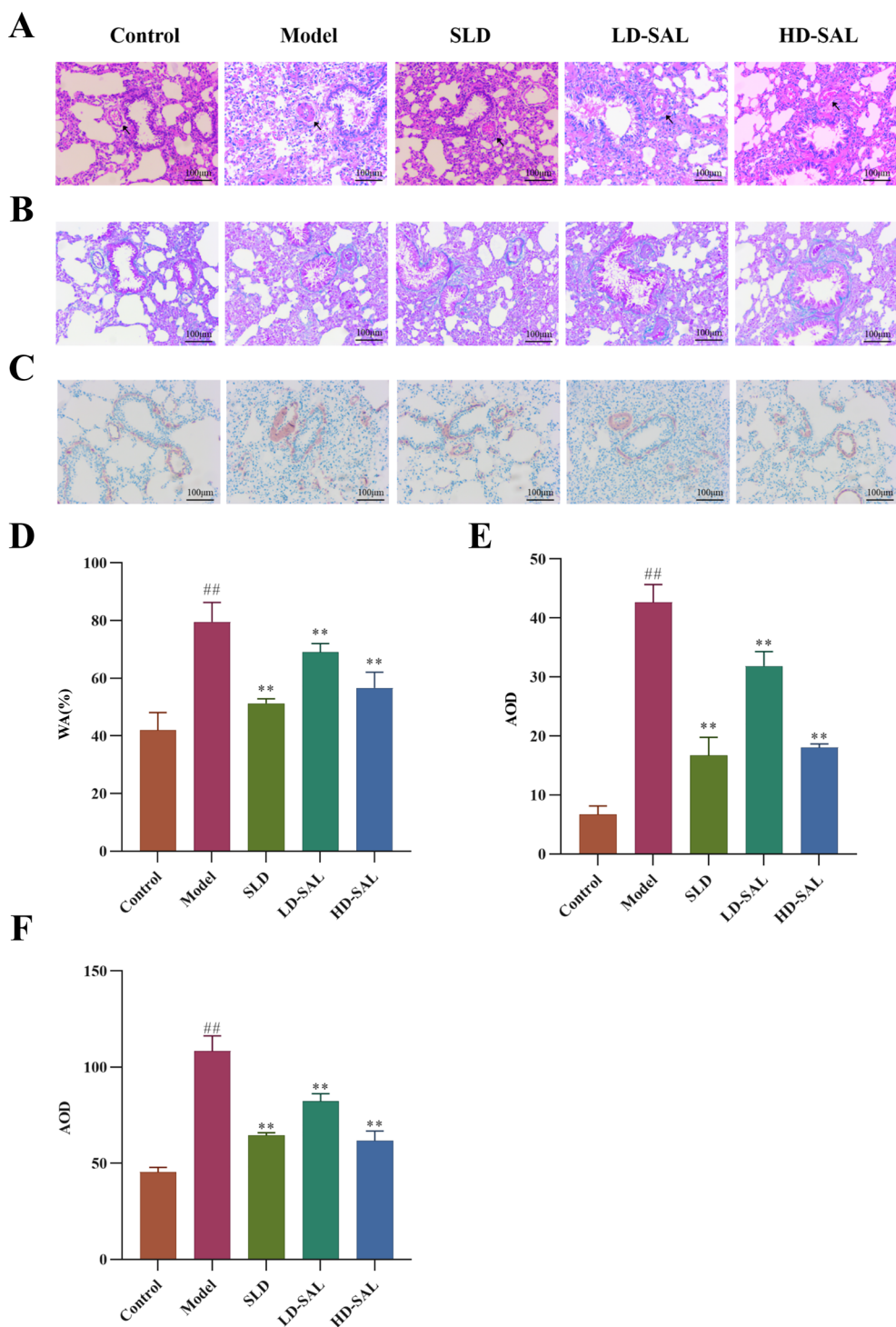


Fig. 2 Salidroside (SAL) treatment ameliorates pulmonary vascular remodeling in MCT-induced PAH rats. **A** Representative images of H&E-stained lung sections (100 \times magnification). **B** Representative images of Masson's trichrome-stained lung sections (100 \times magnification). **C** Representative images of α -SMA immunostaining in lung sections (100 \times magnification). **D** Quantification of wall area percentage (WA%). **E** Quantification of collagen deposition by Masson's trichrome staining (area optical density, AOD). **F** Quantification of α -SMA expression (AOD). Data are presented as mean \pm SD ($n=3$ per group). One-way ANOVA with Tukey's post hoc test was used for statistical analysis. ** $P<0.01$ vs Model group; ## $P<0.01$ vs Control group

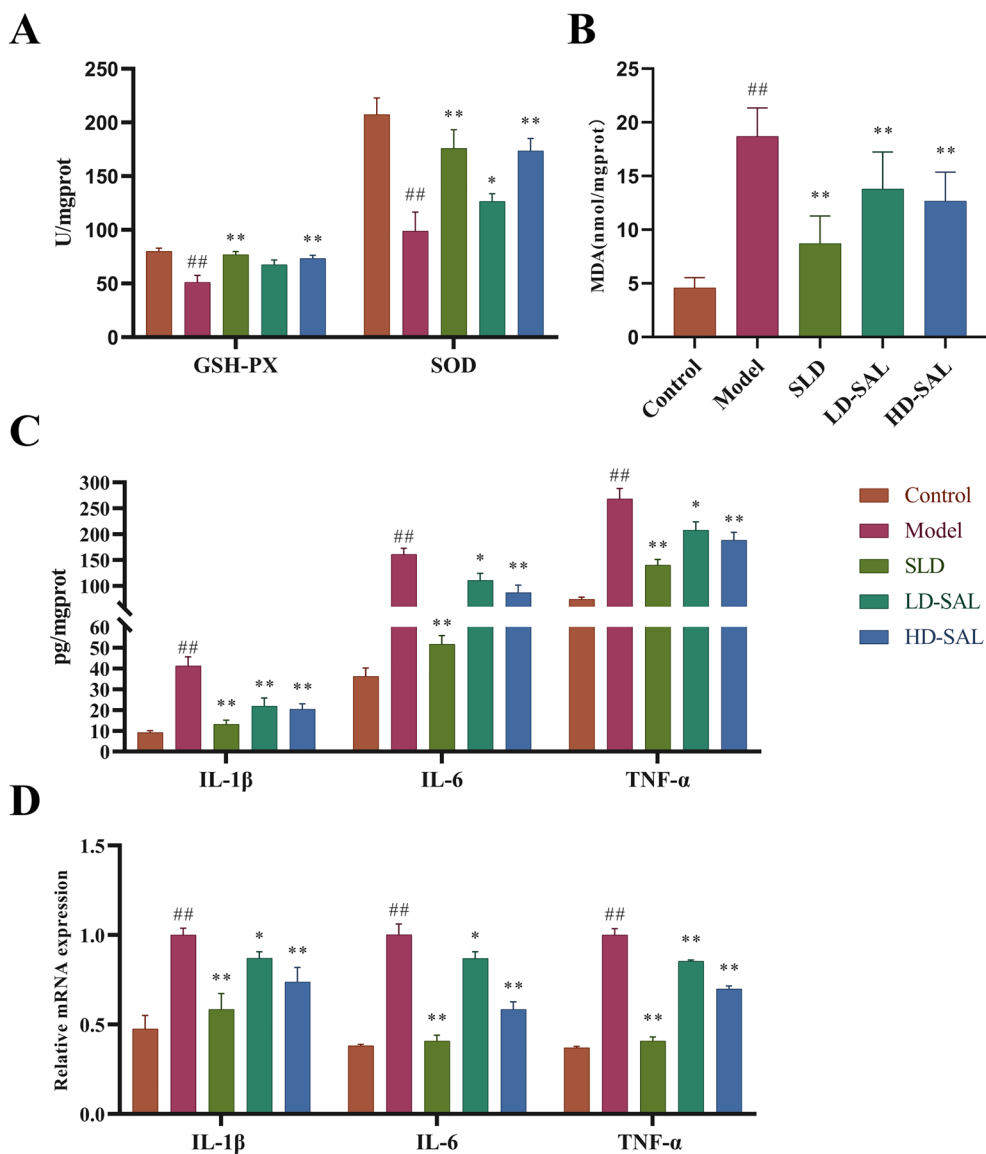


Fig. 3 Salidroside (SAL) treatment improves oxidative stress and inflammatory response in PAH model rats. **A** SAL treatment increased the levels of SOD and GSH-PX. **B** SAL treatment decreased MDA levels. **C** Expression of IL-1 β , IL-6, and TNF- α in lung tissues. **D** Gene transcription of IL-1 β , IL-6, and TNF- α in lung tissues. Data are presented as mean \pm SD ($n=6$ for A–C, $n=3$ for D). One-way ANOVA with Tukey's post hoc test was used for statistical analysis. * $P<0.05$, ** $P<0.01$ vs Model group; ## $P<0.01$ vs Control group

and HD-SAL groups. These pathways included arginine (Arg), proline, citrate, aminoacyl-tRNA, glycerophospholipid, riboflavin, and serine metabolism pathways. Notably, the Arg metabolic pathway is the sole pathway mediating endogenous NO synthesis. The results of the study indicate that SAL significantly ameliorates Arg metabolism disorders, which may be a key mechanism underlying its regulation of eNOS and promotion of NO synthesis and bioavailability (Fig. 5F, G, Table 2).

Discussion

SAL, a key bioactive component derived from the traditional Chinese medicine Rhodiola rosea, has garnered significant attention for its potential therapeutic benefits in various diseases. Recent studies have highlighted the efficacy of both Rhodiola rosea extract and SAL in attenuating PAH and vascular remodeling in preclinical models [9, 12–14]. However, the precise mechanism precisely elucidated. This study provides novel insights into the therapeutic potential of SAL in PAH, demonstrating

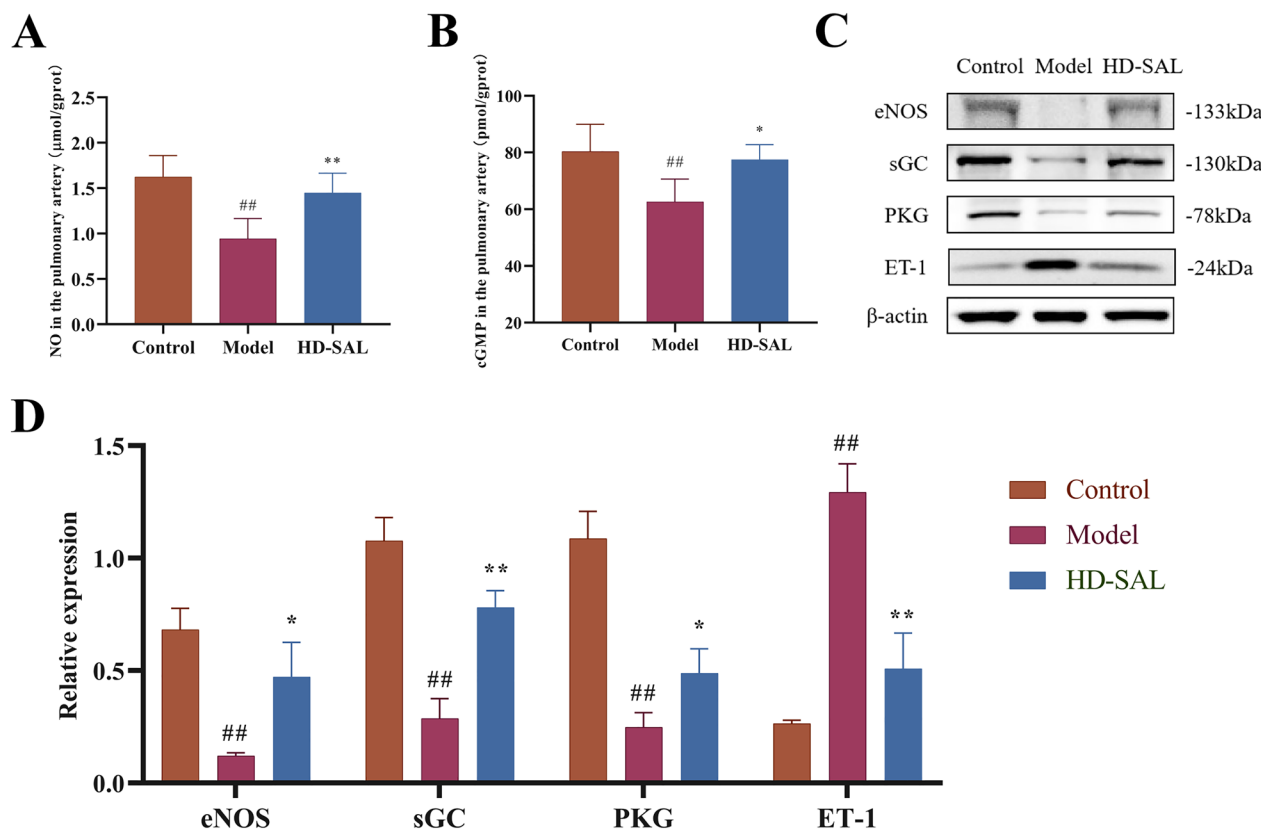


Fig. 4 Salidroside (SAL) treatment enhances NO synthesis and bioavailability in the pulmonary arteries of MCT-induced PAH rats. **A** eNOS protein expression and NO levels in pulmonary artery homogenates. **B** cGMP levels in pulmonary artery homogenates. **C** Representative Western blots showing the protein expression of eNOS, sGC, PKG, and ET-1 in pulmonary arteries. **D** Quantification of Western Blot data. Data are presented as mean \pm SD ($n=6$ for A–B, $n=3$ for D). One-way ANOVA with Tukey's post hoc test was used for statistical analysis. * $P<0.05$ vs Model; ** $P<0.01$ vs Model; ## $P<0.01$ vs Control

its ability to mitigate pulmonary vascular remodeling, oxidative stress, inflammation, and Arg metabolic dysregulation, ultimately leading to enhanced NO bioavailability and reduced pulmonary artery pressure.

Our findings demonstrated that SAL treatment effectively ameliorates MCT-induced PAH in rats, as evidenced by reduced mPAP, improved cardiac function, and attenuated pulmonary vascular remodeling. These results are consistent with previous studies demonstrating the beneficial effects of SAL in various PAH models [9, 12–14]. Importantly, our study goes beyond simply replicating these findings by delving into the potential mechanisms underlying SAL's therapeutic efficacy.

Oxidative stress and inflammatory responses play pivotal roles in the pathogenesis of PAH, contributing to endothelial dysfunction, vascular remodeling, and disease progression [15–19]. Our study found that PAH model rats' lung tissue had oxidative stress and inflammatory responses, consistent with previous studies. SAL intervention significantly increased antioxidant enzymes, reduced MDA, and inhibited pro-inflammatory factors

in PAH model rats' lung tissue. These results suggest that SAL therapeutic benefits in PAH may be partially attributed to its ability to mitigate oxidative stress and inflammation.

NO, the main medium for vasodilation, is critical for vascular homeostasis [20]. Endogenous NO is synthesized and released by eNOS in endothelial cells [21], regulating the sGC-cGMP-PKG pathway in vascular smooth muscle cells for vasodilation [22, 23]. Dysfunctional NO signaling, characterized by reduced eNOS expression and NO bioavailability, is a hallmark of PAH and contributes to vasoconstriction, vascular remodeling, and disease progression [24, 25]. Strategies aimed at restoring NO bioavailability have shown promise in preclinical PAH models [26]. Our study provides compelling evidence that SAL enhances NO synthesis and bioavailability in the pulmonary artery of PAH rats. SAL intervention significantly increased eNOS expression and NO content while also upregulated the sGC-cGMP-PKG pathway and downregulating ET-1 levels. These findings strongly suggest that SAL's therapeutic effects are mediated, at least

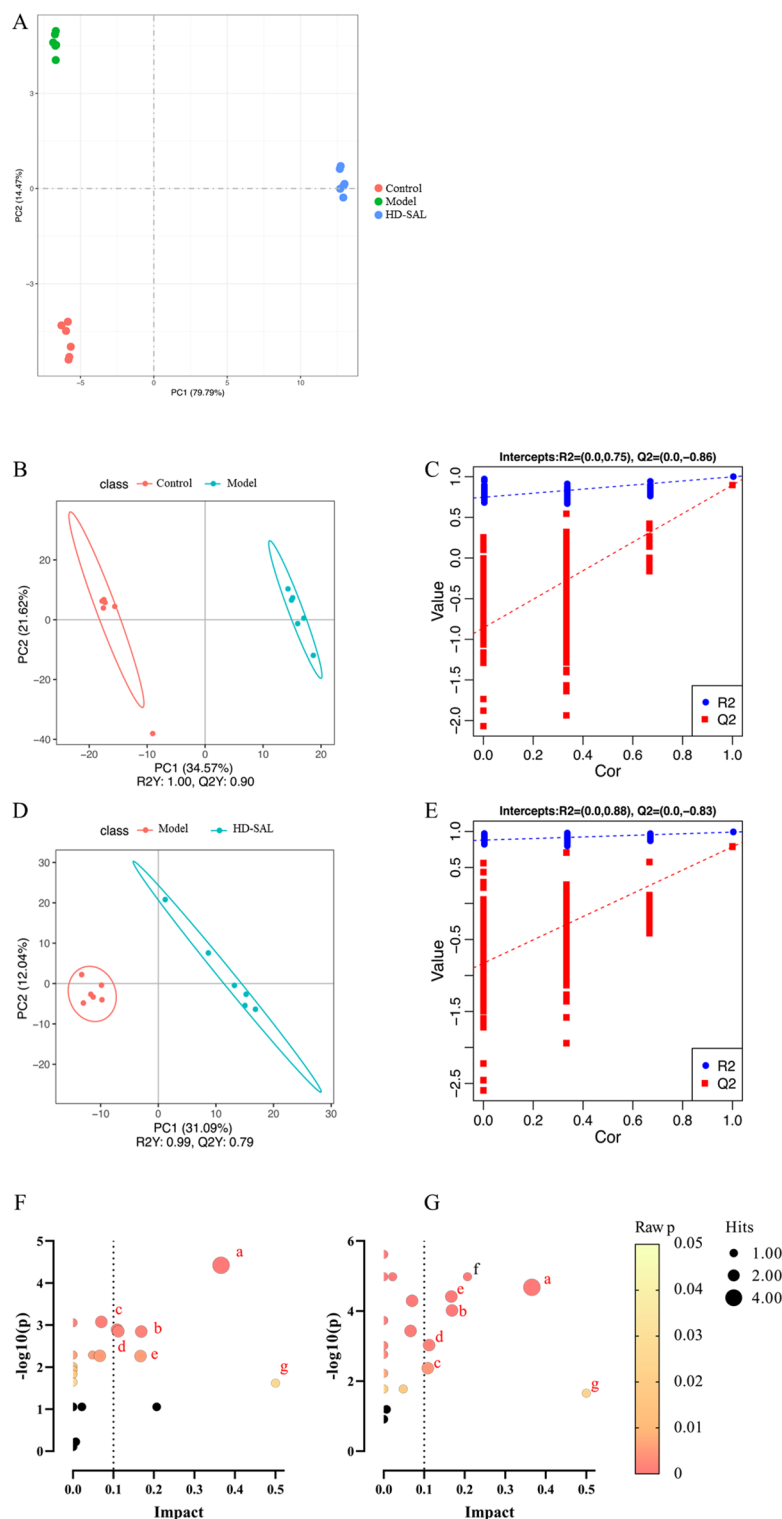


Fig. 5 Salidroside (SAL) treatment modulates metabolic pathways in the pulmonary arteries of MCT-induced PAH rats. **A** PCA score plot for all groups. **B, C** PLS-DA score plot and validation plot for Control vs. Model groups. **D, E** PLS-DA score plot and validation plot for Model vs. HD-SAL groups. **F, G** KEGG pathway enrichment analysis of differentially expressed metabolites in Control vs. Model and Model vs. HD-SAL groups. The pathways include: (a) arginine biosynthesis; (b) arginine and proline metabolism; (c) citric acid cycle (TCA cycle); (d) glycerophospholipid metabolism; (e) aminoacyl-tRNA biosynthesis; (f) serine metabolism; (g) riboflavin metabolism. HD-SAL: high-dose Salidroside. Each group (Control, Model, HD-SAL) consisted of $n=6$ samples

Table 2 Metabolic differential products in the serum of PAH model rats after SAL intervention

No	Formula	RT [min]	m/z	Metabolites		VIP M vs. C	T vs. M	FC M vs. C	T vs. M	M vs. C	T vs. M	Pathway
				Metabolite	Trend							
1	C ₁₁ H ₁₄ N ₂ O ₂	5.17	207.11	1-(4-nitrophenyl)piperidine	1.16	1.01	3.08	2.14	↑##	↑**		
2	C ₁₀ H ₁₀ O ₂	6.05	161.06	1,2-Dihydro-1,2-naphthalenediol	1.68	2.15	0.09	8.87	↓##	↑**		
3	C ₂₀ H ₃₈ O ₂	11.56	309.28	11(E)-Eicosenoic Acid	145	1.36	0.64	1.37	↓##	↑*		
4	C ₂₀ H ₃₄ O ₂	10.56	307.26	11(Z),14(Z),17(Z)-Eicosatrienoic acid	1.17	1.07	0.43	0.57	↓##	↓**		
5	C ₂₀ H ₃₆ O ₆	7.13	371.24	19(R)-Hydroxy prostaglandin F1α	1.36	1.53	1.85	0.59	↑##	↓**		
6	C ₂₃ H ₃₈ O ₅	6.73	417.26	2-(14,15-Epoxyeicosatetraenoyl) glycerol	1.73	1.07	4.22	0.51	↑##	↓**		
7	C ₁₈ H ₃₀ O ₅	7.88	307.19	2,3-dinor Prostaglandin E1	1.87	1.02	0.19	1.95	↓##	↑**		
8	C ₁₂ H ₁₄ N ₂ O ₂	5.35	219.11	5-Methyl-dl-tryptophan	1.26	2.17	1.42	0.64	↑##	↓**		
9	C ₉ H ₁₅ N ₄ O ₈ P	5.41	337.05	Aica ribonucleotide	1.50	2.41	3.53	0.22	↑##	↓**		
10	C ₅ H ₆ O ₅	1.55	145.01	α-Ketoglutaric acid	1.18	1.07	2.65	0.59	↑##	↓*		
11	C ₂₀ H ₃₀ O ₂	9.73	301.22	cis-5,8,11,14,17-Eicosapentaenoic acid	1.29	1.54	1.27	0.76	↑##	↓**		
12	C ₆ H ₆ O ₆	1.447	173.00917	cis-Aconitic acid	1.21	1.05	0.47	1.53	↓#	↑*	C	
13	C ₆ H ₁₃ N ₃ O ₃	1.38	174.09	Citrulline	1.23	1.52	0.78	1.26	↓#	↑*	a	
14	C ₉ H ₁₃ N ₃ O ₅	1.45	266.07	Cytidine	1.40	1.41	1.32	0.77	↑##	↓**		
15	C ₂₄ H ₄₀ O ₄	7.41	391.29	Deoxycholic acid	1.33	1.67	3.88	0.20	↑#	↓*		
16	C ₂₈ H ₄₄ O	8.00	397.34	Ergocaliferol	1.90	1.07	0.22	1.83	↓##	↑*		
17	C ₂₈ H ₄₂ O	7.96	395.33	Ergosta-5,7,9(11),22-Tetraen-3-beta-Ol	1.85	1.58	0.12	3.92	↓##	↑**		
18	C ₈ H ₁₄ O ₇	2.77	221.07	Ethyl-β-D-glucuronide	1.95	1.54	7.20	0.30	↑##	↓*		
19	C ₄₀ H ₇₀ O ₄	10.81	613.52	Fatty acid esters of hydroxy fatty acid (22:4/18:0)	1.03	1.02	0.36	0.46	↓##	↓*		
20	C ₉ H ₉ NO ₃	5.49	178.05	Hippuric acid	1.48	2.67	0.09	29.10	↓##	↑**		
21	C ₆ H ₁₄ N ₄ O ₂	5.17	175.12	Larginine	1.23	1.32	0.60	2.01	↓##	↑**	a,b,e	
22	C ₅ H ₁₂ N ₄ O ₃	3.96	177.10	L-Canavanine	1.60	1.13	0.61	1.31	↓##	↑*		
23	C ₅ H ₁₂ N ₂ O ₂	1.19	133.10	L-Ornithine	1.23	2.36	2.17	0.31	↑##	↓**	a,b	
24	C ₂₆ H ₄₆ NO ₇ P	8.52	516.31	Lysophosphatidylcholine (18:4)	1.40	1.25	2.35	0.53	↑#	↓*	d	
25	C ₂₀ H ₄₂ NO ₇ P	9.23	438.26	Lysophosphatidyl ethanolamine (15:0)	1.18	1.84	1.71	0.53	↑#	↓**		
26	C ₂₂ H ₄₆ NO ₇ P	10.01	468.31	Lysophosphatidylcholine (17:0)	1.30	1.76	1.45	0.67	↑##	↓**		
27	C ₁₁ H ₁₃ NO ₄	5.28	222.08	N-Acetyl-L-tyrosine	1.52	1.20	2.44	0.53	↑##	↓**		
28	C ₄₂ H ₈₂ NO ₇ P	11.50	744.59	phosphatidylcholine (14:0e/20:2)	1.49	2.07	0.50	2.09	↓##	↑**	d	
29	C ₂₅ H ₅₂ NO ₇ P	10.13	510.36	phosphatidylcholine (14:0e/3:0)	1.14	1.65	1.48	0.64	↑##	↓**	d	
30	C ₄₆ H ₈₆ NO ₈ P	10.18	812.61	phosphatidylcholine (18:0/20:3)	1.11	1.52	0.80	1.26	↓#	↑*	d	
31	C ₄₀ H ₈₀ NO ₇ P	10.92	718.58	phosphatidylcholine (18:0e/14:1)	1.66	1.02	0.59	1.27	↓##	↑*	d	
32	C ₄₄ H ₉₄ NO ₈ P	10.82	786.60	phosphatidylcholine (8:1/7:8:1)	1.53	1.65	0.61	1.51	↓##	↑*	d	
33	C ₁₇ H ₂₀ N ₄ O ₆	5.46	377.15	Riboflavin	1.32	1.81	0.66	1.58	↓##	↑*	g	
34	C ₁₆ H ₂₆ O ₃	7.76	265.18	12-hydroxy-5,8,10,14-eicosatetraenoic acid	1.52	1.21	2.26	0.50	↑#	↓**		

Table 2 (continued)

No	Formula	RT [min]	m/z	Metabolites	VIP		FC		Trend		Pathway
					M vs. C	T vs. M	M vs. C	T vs. M	M vs. C	T vs. M	
35	C ₁₀ H ₁₂ N ₄ O ₆	4.79	283.07	Xanthosine	1.60	2.26	2.39	0.40	↑##	↓**	
36	C ₃₈ H ₄₄ NO ₉ P	11.96	568.27	Lipopolyssaccharides (22:6)	1.02	1.77	1.50	0.56	↑	↓**	
37	C ₃ H ₇ NO ₃	1.31	104.04	L-Serine	1.15	2.07	0.49	2.43	→	↑**	f,e
38	C ₃₃ H ₄₆ N ₄ O ₆	5.78	595.35	Stercobilin	1.06	1.76	0.16	6.77	→	↑*	
39	C ₁₅ H ₁₂ I ₃ NO ₄	5.43	649.78	Triiodothyronine	1.09	1.72	0.49	2.05	→	↑**	

RT Retention Time, VIP Variable importance in Projection, FC Fold Change

Compared to the control group $p < 0.05$, ## Compared to the control group $p < 0.01$; * Compared to the model group $p < 0.01$; ** Compared to the model group $p < 0.05$. ↑ Indicates an increase in content, ↓ Indicates a decrease in content; C: Control group; M: Model group; T: High-Dose Salidroside (HD-SAL) group. (a) Arginine biosynthesis; (b) Citric acid cycle (TCA cycle); (d) Glycerophospholipid metabolism; (e) Aminoacyl-tRNA biosynthesis; (f) Glycine, serine, and threonine metabolism; (g) Riboflavin metabolism. Control group, Model group, HD-SAL group, each group n = 6, with a t test. The data were denoted as mean ± SD. * $P < 0.05$, ** $P < 0.01$ vs. Model; # < 0.05 vs. Control, ## $P < 0.01$ vs. Control.

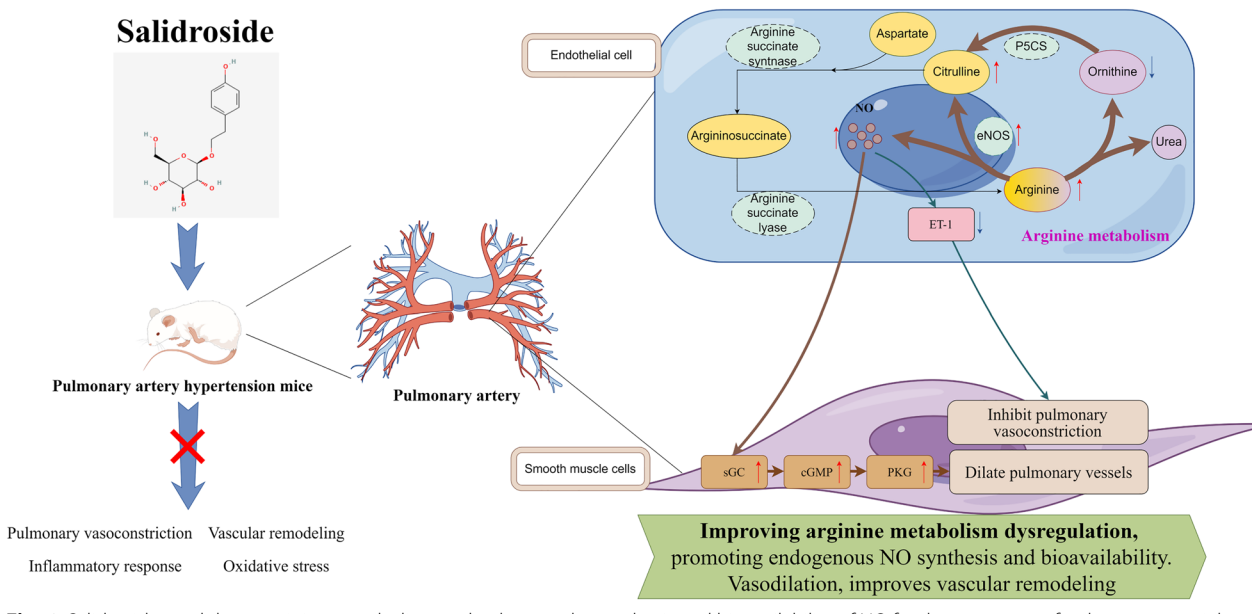


Fig. 6 Salidroside modulates arginine metabolism and enhances the synthesis and bioavailability of NO for the treatment of pulmonary arterial hypertension

in part, by its ability to restore NO signaling in the pulmonary vasculature.

Furthermore, our untargeted metabolomics analysis revealed a novel mechanism by which SAL may exert its beneficial effects in PAH. We observed that Arg metabolism, the citric acid cycle, amino acid-tRNA synthesis, glycerophospholipid metabolism, riboflavin metabolism, and serine metabolism were related pathways with significant differences in metabolites between the Model group and SAL group. Among these, the Arg metabolic pathway has been confirmed to be closely related to the endogenous NO synthesis and bioavailability in PAH [27].

Arg is the sole precursor of endogenous NO, and its reduced content limits endogenous NO synthesis [28]. eNOS catalyzes Arg to produce NO and Citrulline (Cit), forming an Arg-Cit cycle to continuously synthesizing NO *in vivo* [29]. Arg can also be catabolized into urea and ornithine (Orn) under arginase [30], and Orn can achieve the conversion between Arg and glutamate through pyrrolidine-5-carboxylate synthetase (P5CS) mediation [31]. α -Ketoglutaric acid (α -KG) is produced after glutamate dehydrogenase transformation to participate in the TAC cycle, thereby providing energy for cell metabolism in PAH and accelerating pulmonary vascular remodeling [32]. Previous studies confirmed decreased plasma Arg and Cit levels and the Arg/Orn ratio in PAH patients [29, 33]. The imbalance of Arg metabolism is the key reason for promoting PAH development [27]. Our research found disturbed Arg metabolism pathway in the pulmonary arteries of PAH rats, shown as decreased Arg and

Cit levels and increased Orn and α -KG levels. These metabolic alterations suggest a shift in Arg metabolism away from NO synthesis and towards citric acid cycle, potentially contributing to reduced NO synthesis and bioavailability. Importantly, SAL treatment partially restored Arg metabolic balance, suggesting that its ability to enhance NO synthesis and bioavailability may be linked to its modulatory effects on Arg metabolism (Fig. 6).

While our study provides compelling evidence for the therapeutic potential of SAL in PAH, it is not without limitations. The use of a single dose of MCT to induce PAH, while a widely used model, may not fully recapitulate the complexity of human PAH. Further studies using alternative PAH models and investigating the long-term effects of SAL treatment are warranted. Additionally, while our metabolomics analysis identified significant alterations in Arg metabolism, further investigation is needed to elucidate the precise molecular mechanisms by which SAL modulates this pathway. Specifically, future studies should investigate the potential involvement of the DDAH-1-ADMA-eNOS pathway [34, 35] and the role of Nrf-2 [36], a transcription factor known to be upregulated by SAL [37], in mediating these effects.

Conclusion

This study provides compelling evidence for the therapeutic potential of SAL in PAH. SAL effectively attenuates pulmonary vascular remodeling, oxidative stress, and inflammation, and enhances NO synthesis and bioavailability, potentially by modulating the

Arg metabolic pathway. These findings warrant further investigation into the clinical utility of SAL as a novel therapeutic strategy for PAH.

Supplementary Information

The online version contains supplementary material available at <https://doi.org/10.1186/s40001-024-02016-x>.

- Supplementary Material 1
- Supplementary Material 2
- Supplementary Material 3
- Supplementary Material 4
- Supplementary Material 5

Acknowledgements

Not applicable.

Author contributions

Conceptualization, Junfei Li and Hongyan Zhang; methodology, Junfei Li, Chenghui Zhu and Zengyu Zhang; investigation, Junfei Li and Jianwei Jiang; data curation, Chenghui Zhu, Jianwei Jiang, Xiaorong Zheng and Chunlei Wang; writing-original draft preparation, Junfei Li, Chenghui Zhu and Zengyu Zhang; writing-review and editing, Junfei Li and Hongyan Zhang; supervision, Jianwei Jiang and Hongyan Zhang; funding acquisition, Junfei Li. All authors have read and agreed to the published version of the manuscript.

Funding

This work was supported by the "Zhejiang Pharmaceutical Association" under Grant No. 2021zyy17 and the "Zhejiang Traditional Chinese Medicine Administration" under Grant No. 2021ZZ006 and the "Medical Science and Technology Project of Zhejiang Province" under Grant No. 2020KY074. The funders had no role in study design, data collection and analysis, decision to publish, or preparation of the manuscript.

Availability of data and materials

The raw data of the vitro/in vivo experiments and all bioinformatics analysis are available in the Supplementary Files. Data is provided within the manuscript or supplementary information files.

Declarations

Ethics approval and consent to participate

Animal treatment and maintenance were performed in accordance with the Principles of Laboratory Animal Care (NIH Publication no.85–23, revised 1985). All procedures for animal care and experiments were reviewed and approved by the Zhejiang Cancer Hospital Animal Ethical Committee (No. zjzlsd 2023–07–088).

Consent for publication

Not applicable.

Competing interests

The authors declare no competing interests.

Received: 13 May 2024 Accepted: 7 August 2024

Published online: 17 August 2024

References

1. Humbert M, Kovacs G, Hoeper MM, et al. 2022 ESC/ERS guidelines for the diagnosis and treatment of pulmonary hypertension. *Eur Respir J*. 2023;61(1):2200879.
2. Marra AM, Sherman AE, Ameri P, Bossone E. Challenges in pulmonary hypertension. *Heart Fail Clin*. 2023;19(1):xv–xvi.
3. Suliman HB, Nozik-Grayck E. Mitochondrial dysfunction: metabolic drivers of pulmonary hypertension. *Antioxid Redox Signal*. 2019;31(12):843–57.
4. Zuchi C, Tritto I, Carluccio E, Mattei C, Cattadori G, Ambrosio G. Role of endothelial dysfunction in heart failure. *Heart Fail Rev*. 2020;25(1):21–30.
5. Arai MA, Sakuraba K, Makita Y, Hara Y, Ishibashi M. Evaluation of naturally occurring HIF-1 inhibitors for pulmonary arterial hypertension. *ChemBioChem*. 2021;22(18):2799–804.
6. Sun S, Tuo Q, Li D, et al. Antioxidant effects of salidroside in the cardiovascular system. *Evid Based Complement Alternat Med*. 2020;2020:9568647.
7. Leung SB, Zhang H, Lau CW, Huang Y, Lin Z. Salidroside improves homocysteine-induced endothelial dysfunction by reducing oxidative stress. *Evid Based Complement Alternat Med*. 2013;2013:679635.
8. Xing SS, Yang XY, Zheng T, et al. Salidroside improves endothelial function and alleviates atherosclerosis by activating a mitochondria-related AMPK/Pi3K/Akt/eNOS pathway. *Vascul Pharmacol*. 2015;72:141–52.
9. Huang X, Zou L, Yu X, et al. Salidroside attenuates chronic hypoxia-induced pulmonary hypertension via adenosine A2a receptor related mitochondria-dependent apoptosis pathway. *J Mol Cell Cardiol*. 2015;82:153–66.
10. Chen M, Cai H, Yu C, et al. Salidroside exerts protective effects against chronic hypoxia-induced pulmonary arterial hypertension via AMPKa1-dependent pathways. *Am J Transl Res*. 2016;8(1):12–27.
11. Arifin WN, Zahiruddin WM. Sample size calculation in animal studies using resource equation approach. *Malays J Med Sci*. 2017;24(5):101–5.
12. Nan X, Su S, Ma K, et al. Bioactive fraction of Rhodiola algida against chronic hypoxia-induced pulmonary arterial hypertension and its anti-proliferation mechanism in rats. *J Ethnopharmacol*. 2018;216:175–83.
13. Nan X, Yang Z, Su S, et al. The Mechanism of Volatile Oil of rhodiola tangutica against Hypoxia-Induced Pulmonary Hypertension in Rats Based on RAS Pathway. *Biomed Res Int*. 2022;2022:9650650.
14. Ren HH, Niu Z, Guo R, et al. Rhodiola crenulata extract decreases fatty acid oxidation and autophagy to ameliorate pulmonary arterial hypertension by targeting inhibiton of acylcarnitine in rats. *Chin J Nat Med*. 2021;19(2):120–33.
15. Pena E, El Alam S, Siques P, Brito J. Oxidative stress and diseases associated with high-altitude exposure. *Antioxidants*. 2022;11(2):267.
16. Reyes-García J, Carbajal-García A, Di Mise A, Zheng YM, Wang X, Wang YX. Important functions and molecular mechanisms of mitochondrial redox signaling in pulmonary hypertension. *Antioxidants*. 2022;11(3):473.
17. Sharma S, Ruffenach G, Umar S, Motayagheni N, Reddy ST, Eghbali M. Role of oxidized lipids in pulmonary arterial hypertension. *Palm Circ*. 2016;6(3):261–73.
18. Sun Y, Chen R, Lin S, et al. Association of circular RNAs and environmental risk factors with coronary heart disease. *BMC Cardiovasc Disord*. 2019;19(1):223.
19. Sun C, Ni M, Song B, Cao L. Circulating circular RNAs: novel biomarkers for heart failure. *Front Pharmacol*. 2020;11:560537.
20. El-Mahdy MA, Ewees MG, Eid MS, Mahgoub EM, Khaleel SA, Zweier JL. Electronic cigarette exposure causes vascular endothelial dysfunction due to NADPH oxidase activation and eNOS uncoupling. *Am J Physiol Heart Circ Physiol*. 2022;322(4):H549–67.
21. López-Preza FI, de la Huerta Cruz S, Santiago-Castañeda C, et al. Hydrogen sulfide prevents the vascular dysfunction induced by severe traumatic brain injury in rats by reducing reactive oxygen species and modulating eNOS and H2S-synthesizing enzyme expression. *Life Sci*. 2023;312:121218.
22. Lázár Z, Mészáros M, Bikov A. The nitric oxide pathway in pulmonary arterial hypertension: pathomechanism, biomarkers and drug targets. *Curr Med Chem*. 2020;27(42):7168–88.
23. Lancaster JR Jr. Historical origins of the discovery of mammalian nitric oxide (nitrogen monoxide) production/physiology/pathophysiology. *Biochem Pharmacol*. 2020;176:113793.
24. Dikalova A, Aschner JL, Kaplowitz MR, Cunningham G, Summar M, Fike CD. Combined L-citrulline and tetrahydrobiopterin therapy improves NO signaling and ameliorates chronic hypoxia-induced pulmonary hypertension in newborn pigs. *Am J Physiol Lung Cell Mol Physiol*. 2020;318(4):L762–72.

25. Gupta RM, Libby P, Barton M. Linking regulation of nitric oxide to endothelin-1: the Yin and Yang of vascular tone in the atherosclerotic plaque. *Atherosclerosis*. 2020;292:201–3.
26. Toxvig AK, Wehland M, Grimm D, Infanger M, Krüger M. A focus on riociguat in the treatment of pulmonary arterial hypertension. *Basic Clin Pharmacol Toxicol*. 2019;125(3):202–14.
27. Hannemann J, Böger R. Dysregulation of the nitric oxide/dimethylarginine pathway in hypoxic pulmonary vasoconstriction—molecular mechanisms and clinical significance. *Front Med*. 2022;9:835481.
28. Chen CL, Hsu SC, Ann DK, Yen Y, Kung HJ. Arginine signaling and cancer metabolism. *Cancers*. 2021;13(14):3541.
29. Scott JA, Maarsingh H, Holguin F, Grasemann H. Arginine therapy for lung diseases. *Front Pharmacol*. 2021;12:627503.
30. Kao CC, Wedes SH, Hsu JW, et al. Arginine metabolic endotypes in pulmonary arterial hypertension. *Pulm Circ*. 2015;5(1):124–34.
31. Colonna MB, Moss T, Mokashi S, et al. Functional assessment of homozygous ALDH1A1 variants reveals alterations in amino acid and antioxidant metabolism. *Hum Mol Genet*. 2023;32(5):732–44.
32. Xu W, Janocha AJ, Erzurum SC. Metabolism in pulmonary hypertension. *Annu Rev Physiol*. 2021;83:551–76.
33. Xu W, Comhair SAA, Chen R, et al. Integrative proteomics and phosphoproteomics in pulmonary arterial hypertension. *Sci Rep*. 2019;9(1):18623.
34. Münz T, Daiber A. Vascular redox signaling, endothelial nitric oxide synthase uncoupling, and endothelial dysfunction in the setting of transportation noise exposure or chronic treatment with organic nitrates. *Antioxid Redox Signal*. 2023;38(13–15):1001–21.
35. Wang D, Li H, Weir EK, Xu Y, Xu D, Chen Y. Dimethylarginine dimethylaminohydrolase 1 deficiency aggravates monocrotaline-induced pulmonary oxidative stress, pulmonary arterial hypertension and right heart failure in rats. *Int J Cardiol*. 2019;295:14–20.
36. Nair N, Gongora E. Oxidative stress and cardiovascular aging: interaction between NRF-2 and ADMA. *Curr Cardiol Rev*. 2017;13(3):183–8.
37. Lu H, Li Y, Zhang T, et al. Salidroside reduces high-glucose-induced podocyte apoptosis and oxidative stress via upregulating heme oxygenase-1 (HO-1) expression. *Med Sci Monit*. 2017;23:4067–76.

Publisher's Note

Springer Nature remains neutral with regard to jurisdictional claims in published maps and institutional affiliations.